THE JOURNAL OF PHYSICAL CHEMISTRY B

Article

pubs.acs.org/JPCB

Binary *n*-Alkane Mixtures from Total Miscibility to Phase Separation in Microcapsules: Enrichment of Shorter Component in Surface Freezing and Enhanced Stability of Rotator Phases

Dongsheng Fu, Yufeng Liu, Xia Gao, Yunlan Su,* Guoming Liu, and Dujin Wang*

Beijing National Laboratory for Molecular Sciences, Key Laboratory of Engineering Plastics, Institute of Chemistry, Chinese Academy of Sciences, Beijing 100190, China

ABSTRACT: The crystallization behaviors of binary normal alkane (*n*-alkane) mixtures with a series of carbon number difference (denoted as Δn), both in the bulk state and in nearly monodisperse microcapsules, have been investigated by the combination of differential scanning calorimetry (DSC) and temperature-dependent X-ray diffraction (XRD). As revealed by the DSC data, the surface freezing temperature (denoted as T_s) of spatially confined binary *n*-alkane mixtures with large Δn is lower than the calculated value due to the enrichment of shorter component in the surface freezing phase. More alkane molecules with shorter carbon chain are located on the interface between the inner shell of microcapsules and the bulk mixture, thus leading to the decrease of the average chain length of the surface freezing phase and corresponding lower T_s. Furthermore, XRD results have proved that the enhanced surface freezing phenomenon can contribute to the stabilization of the rotator phases in *n*-alkane mixtures and even induce the crossover of some certain rotator phase (RII) from transient to metastable. However, the decisive reason for such stabilization or crossover is attributed to the suppression of the orienting movement of alkane molecules toward their next-nearest neighbors within the layer of rotator phases.

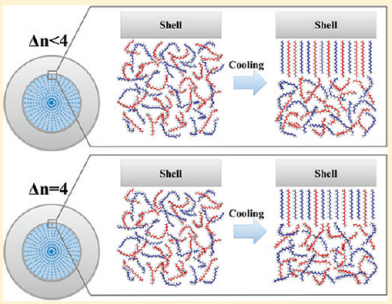

INTRODUCTION

In the past three decades, *n*-alkanes and *n*-alkane mixtures have been extensively investigated. Since the linear chains of saturated hydrocarbons virtually act as the most fundamental organic series, *n*-alkanes can provide well-defined model for studying the complex crystallization behavior of polymer materials, surfactants, and lipids.[1] Moreover, a representative application is that once encapsulated, *n*-alkane mixtures have been proved to be superior as phase change materials (PCMs) for thermal protection and energy storage.[2,3] Several unique features have been found and extensively studied, one of which is surface freezing. Surface freezing is a kind of crystallization behavior emerging above the bulk freezing temperature, which has been observed in some liquid crystals,[4,5] normal alkanes (*n*-alkanes),[6,7] normal alcohols,[8,9] and even surfactant molecules on the O/W interface.[10,11] The surface molecules of those materials will first freeze before the bulk crystallization under some certain conditions. Among those materials above, the surface freezing of *n*-alkanes has been investigated in detail. Many special methods were used for the research of surface freezing, such as X-ray reflection, X-ray grazing incidence diffraction, and surface tension measurements, and the combination of these techniques has successfully detected solid features on the vapor−liquid interface while the bulk alkane is still in liquid state.[12−18] It has been further revealed that the surface freezing phase of single *n*-alkanes is a two-dimensional (2-D) monolayer, in which alkane molecules are hexagonally arranged.[6] This kind of peculiar crystallization behavior in *n*-alkanes is probably due to the methyl end with low surface energy or long chain geometrical form of *n*-alkanes.[19] Another possible reason has also been put forward that surface freezing can be entropically stabilized by fluctuations along the axis of the molecules.[20] The similar surface freezing phenomenon has also been detected in binary *n*-alkane mixtures adopting the same structure as that of single *n*-alkanes. However, when carbon number difference (denoted as Δn) is large, the longer component is prone to stay on the interface, while the phase separation is not found in the surface freezing phase.[21,22] Furthermore, the surface freezing phase of *n*-alkanes is intimately related to the formation of solid phases in *n*-alkanes and *n*-alkane mixtures.[23] Some metastable solid phases can be induced by the surface freezing phase, and the nucleation velocity can be significantly increased during the cooling process.[24] The existence of the surface freezing phase can lower the interface tension between the matrixes and the newly born nucleates and promote the formation and stabilization of solid phases.[25,26] Therefore, the research on surface freezing in *n*-alkanes can offer great help to the explanation and understanding for the phase behaviors of liquid crystal or other complex materials with the similar structure.

Another frequently referenced feature for *n*-alkane crystallization is the formation of rotator phases, which exist in the temperature region between isotropic liquid phase and low-temperature ordered crystal phase.[27,28] The gauche conformation emerges in the alkane molecules of these rotator phases,

Received: December 27, 2011
Revised: February 10, 2012
Published: February 15, 2012

   dx.doi.org/10.1021/jp2125119 | *J. Phys. Chem. B* 2012, 116, 3099−3105

Table 1. Molecular Characteristics of Binary *n*-Alkane Mixtures[a]

Δn	1		2		3		4			
components	C_{18}	C_{19}	C_{18}	C_{20}	C_{18}	C_{21}	C_{18}	C_{22}	C_{17}	C_{21}
m/g	0.5	0.5	0.5	0.5	0.5	0.5	0.5	0.5	0.5	0.5
$n/\times10^{-3}$ mol	1.97	1.86	1.97	1.77	1.97	1.69	1.97	1.61	2.08	1.69
$\varphi_n \times 100\%$	51.4	48.6	52.7	47.3	53.8	46.2	55.0	45.0	55.2	44.8
$\bar{n}$	18.49		18.95		19.39		19.80		18.79	

[a] Δn: carbon number difference; φ_n: molar fraction of each component; $\bar{n}$: average chain length.

and hence the rotator phase lacks long-range order in the rotational degree of freedom of the molecules around their long axis, only exhibiting long-range order in the molecular axis orientation and the center of mass position.[29−31] For *n*-alkane mixtures, the temperature region of rotator phases is relatively enlarged, showing an increasing stability of rotator phases due to favorable miscibility.[32]

It has been well-known that phase transitions can be dramatically affected by the size effect, such as the unusual phase behaviors of spatially confined films or other soft matters.[33−43] As a sort of phase transition, surface freezing can also be influenced by finite geometry, especially in the very small space. The specific surface area is sharply enlarged, and the amount of molecules on the surface or interface will be greatly increased. Therefore, surface freezing is expected to be enhanced, which has been confirmed by the situations observed in the microcapsule prepared by the *in situ* polymerization method, using the melamine−formaldehyde resin as shell materials.[44−46] Such microcapsules can provide a stable three-dimensional (3-D) confinement for *n*-alkanes or *n*-alkane mixtures as core materials.[47−49] Since the geometry size is reduced to micrometer, the specific surface area for the inner wall of microcapsules is prominently enlarged, and the proportion of alkane molecules on the interface increases to almost 1% of the whole molecules, leading to the enhanced surface freezing.[44] In bulk *n*-alkanes, normal measurements fail to detect the transition enthalpy due to small amount of surface molecules. In microcapsules, however, since the amount of alkane molecules on the interface is greatly increased, the enthalpy of the surface freezing transition can be detected by normal DSC methods characterized by a small exothermic peak preceding the liquid−solid phase transition during the cooling process.[44−46,50−53] In addition, the enhanced surface freezing can promote the stabilization of rotator phases and even contribute to the crossover of some certain rotator phase from a transient phase to a metastable one.[44,45,53] The hexagonally packed rotator phase II (abbreviated as RII), originally found in pure *n*-alkanes (C_{22}−C_{26}) and binary alkane mixtures containing one or two of the above *n*-alkanes, was observed in the microencapsulated C_{19} (m-C_{19})[44] and C_{18}/C_{20} (m-C_{18}/C_{20}) under all concentrations.[53] It is believed that with the same in-planar structure as RII the surface freezing monolayer acts as the perfect nucleating sites for bulk crystallization of *n*-alkanes or *n*-alkane mixtures, and hence the interface tension and energy are greatly reduced, leading to the RII crossover.[44] All the above-mentioned investigations are mainly focused on single alkanes and binary mixtures with good solubility. Up to date, however, little attention has been paid to the binary alkane mixtures with poor solubility even near to phase separation. The enlargement of Δn results in larger repulsive effect between two components, and phase separation is apt to emerge.[54−56] Furthermore, the formation mechanism of RII has not been thoroughly investigated. Therefore, one can expect fascinating results on the confined surface freezing phenomenon and the formation of subsequent rotator phases when the two components of binary mixtures become more and more insoluble.

In our former works, the phase transition and phase separation behaviors of confined binary *n*-alkane mixtures (m-C_{18}/C_{19},[50,51] m-C_{18}/C_{20}[52,53]) have been studied, and the microcapsule has been proved to be a stable unique 3-D confinement for the research on the phase behaviors of binary *n*-alkane mixtures. In the present investigation, we mainly focus on the crystallization of binary *n*-alkane mixtures (with different Δn) both in the bulk state and in microcapsules. The similar enhanced surface freezing phenomenon is detected by DSC measurements, and the surface freezing temperature (denoted as T_s) of the *n*-alkane mixture with large Δn deviates from the calculation. XRD results show that when Δn becomes larger, the metastable temperature region of RII is constantly enlarged, showing a growing stability of RII. Moreover, the effect of molecular repulsion between the components on the stability of rotator phases will be discussed on the basis of the experimental observations.

EXPERIMENTAL METHODS

n-$C_{17}H_{36}$ (purity >99%), *n*-$C_{18}H_{38}$ (purity >99%), *n*-$C_{19}H_{40}$ (purity >99%), *n*-$C_{20}H_{42}$ (purity >99%), *n*-$C_{21}H_{44}$ (purity >98%), and *n*-$C_{22}H_{46}$ (purity >99%) were purchased from Acros or Sigma-Aldrich Company, and all compounds were used as received. Several combinations of binary *n*-alkane mixtures with different Δn were designed, and the mass fraction of all components was fixed by 50%. If φ_n is the molar fraction of chain length *n*, where $\sum_n \varphi_n = 1$, then $\bar{n} = \sum_n \varphi_n n$. The corresponding molar fraction φ_n and average chain length (denoted as $\bar{n}$) were calculated and shown in Table 1. The solid bulk components were weighted in the desired mass fraction and melt-mixed. Using melamine−formaldehyde (M-F) resin as the shell material and *n*-alkane mixtures as the core material, microcapsules were prepared by *in situ* polymerization according to literatures.[47−49] This method provides us with nearly monodisperse and highly heat-resistant microcapsules, inside which *n*-alkane mixtures are confined to individually small microdomains surrounded by the noncrystalline wall of M-F resin.

The particle size and surface morphology of the prepared microcapsules were examined by a JEOL-JSM-6700F scanning electron microscope (SEM) (Figure 1), fitted with a field emission source and operated at an accelerating voltage of 5 kV. The differential scanning calorimetry (DSC) measurements were carried out on a Perkin-Elmer DSC7 calorimeter at a cooling/heating rate of 2 °C/min. Specimens were heated from room temperature to 45 °C and then cooled down to −10 °C, followed by heating again to 45 °C. The first cooling and second heating thermograms were recorded.

Temperature-dependent X-ray diffraction (XRD) experiments were performed on an X'Pert Pro MPD X-ray diffractometer over the temperature region from −10 to 40 °C, using

dx.doi.org/10.1021/jp2125119 | J. Phys. Chem. B 2012, 116, 3099−3105

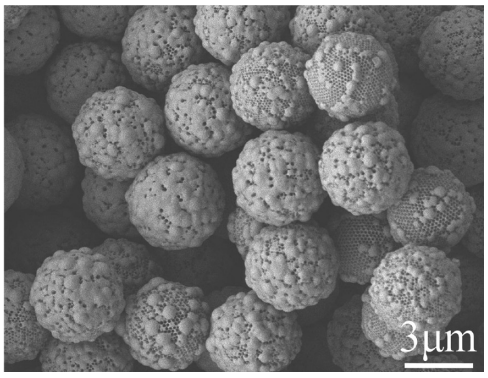

Figure 1. SEM images of microcapsules prepared by *in situ* polymerization using melamine–formaldehyde as shell materials and *n*-alkane mixtures as core materials. The emulsifier is 4-(1,1,3,3-tetramethylbutyl)phenylpoly(ethylene glycol) (Triton X-100), and the reaction temperature is 70 °C.

Cu Kα radiation (1.54 Å), power of 40 mA/40 kV, and rotating angle $2\theta = 5°–40°$. The samples with thickness of about 1 mm were enclosed in aluminum foil, first heated from room temperature to 40 °C, kept for 5 min, and followed by cooling to −10 °C. The heating and cooling rates were all 2 °C/min. At each temperature point, the samples were equilibrated for about 5 min before measurements.

RESULTS AND DISCUSSION

Microcapsules with a mean diameter of ca. 3.5 μm are nearly monodisperse with surface porous morphology (Figure 1), and they were utilized in the present paper as the perfect uniform confinement for the confined crystallization of *n*-alkane mixtures. The entire phase transition behaviors in microcapsules during the crystallization process are illustrated using the *m*-C_{18}/C_{20} specimen as an example, as shown in Figure 2.

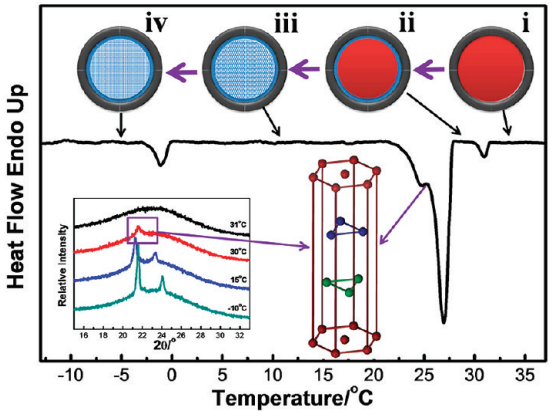

Figure 2. Phase transition behaviors of the microencapsulated C_{18}/C_{20} (*m*-C_{18}/C_{20}) during the cooling process. In the DSC trace, four temperature regions are correspondingly indicated: (i) the isotropic liquid state; (ii) the surface freezing phase coexisting with the liquid phase; (iii) rotator phases (RII or RI); (iv) low-temperature ordered crystal phase. The left inset is the XRD result. The single diffraction peak at $2\theta = 21.6°$ shows the emergence of RII, corresponding to the shoulder exothermic peak in the DSC trace. The 3-D structure of RII is illustrated in the middle inset.

In the DSC trace, four regions are assigned: (i) the isotropic liquid state; (ii) the surface freezing phase coexisting with the liquid phase; (iii) rotator phases; (iv) the low-temperature ordered crystal phase. The single diffraction peak at $2\theta = 21.6°$ in the XRD result (Figure 2, left inset) shows the emergence of RII (Figure 2, middle inset), corresponding to the shoulder exothermic peak in the DSC trace.

Enrichment of Shorter Component in Surface Freezing. Previously, the phase behaviors of C_{18}/C_{20} mixture under all concentrations both in the bulk state and in microcapsules have been discussed in detail.[52,53] The surface freezing temperature (T_s) vary continuously and monotonically with the increase of C_{20} content.[53] Here we substitute the average chain length ($\bar{n}$) of mixtures for the C_{20} content and the similar variance between T_s and $\bar{n}$ is observed (Figure 3a). The linear relationship can be fitted by the equation

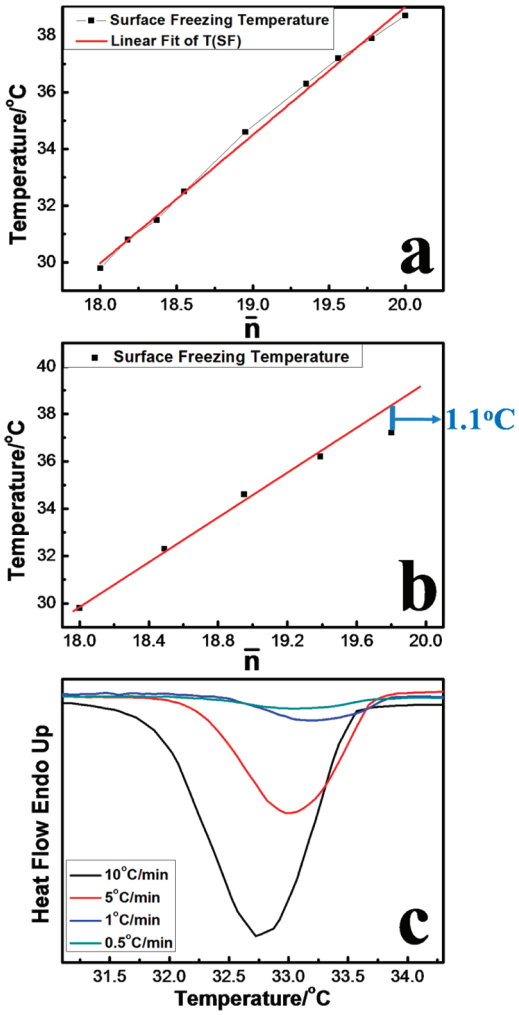

Figure 3. Relations between the average chain length ($\bar{n}$) of the binary *n*-alkane mixtures and the surface freezing temperature in microcapsules: (a) the *m*-C_{18}/C_{20} samples under all concentrations; (b) the binary mixtures with various carbon number difference under equal mass fraction of the two components; (c) the DSC traces of the surface freezing phase under different cooling rates.

$$T_s = 4.52\bar{n} - 51.34 \quad (1)$$

while T_s is the surface freezing temperature and $\bar{n}$ is the average chain length. The two components of C_{18}/C_{20} system are well soluble, and therefore it can be reasonably deduced that once binary *n*-alkane mixtures are composed of two soluble components, T_s under some certain concentration should

dx.doi.org/10.1021/jp2125119 | J. Phys. Chem. B 2012, 116, 3099–3105

correspond to $\bar{n}$ calculated by eq 1. In the present work this equation is used for the investigation on the relations between T_s and $\bar{n}$ in the poorly soluble binary *n*-alkane mixtures. All values of T_s (both calculated and experimental) and $\bar{n}$ are given in Table 2, and the corresponding relation is shown in

Table 2. Surface Freezing Temperature of Binary *n*-Alkane Mixtures[a]

			T_s/°C		
Δn	sample	$\bar{n}$	calcd	exptl	ΔT_s/°C
0	m-C_{18}	18	30.0	29.8	0.2
1	m-C_{18}/C_{19}	18.49	32.3	32.2	0.1
2	m-C_{18}/C_{20}	18.95	34.3	34.5	−0.2
3	m-C_{18}/C_{21}	19.39	36.3	36.2	0.1
4	m-C_{18}/C_{22}	19.80	38.2	37.1	1.1
	m-C_{17}/C_{21}	18.79	33.6	32.9	0.7

[a] Δn: carbon number difference; $\bar{n}$: average chain length T_s: surface freezing temperature; ΔT_s: difference between calculated T_s and experimental T_s. ΔT_s is obtained by calculated T_s minus experimental T_s.

Figure 3b. Obviously, when Δn is small (as for Δn = 1, 2, 3), the two values of T_s are in good agreement, indicating that these samples are composed of well-soluble components. However, the calculated T_s is about 1 °C higher than the experimental one obtained from DSC measurements when Δn = 4. It is known that when Δn becomes larger, the components of binary *n*-alkane mixtures become more repulsive even insoluble, and the solid−solid phase separation will emerge during the cooling process. More energy should be provided to overcome the molecular repulsion of two components; otherwise, they will not coexist in a homogeneous phase, unless the temperature can be further decreased. Therefore, the phase separation can contribute to the deviation of the experimental T_s from the calculated one. However, there is no division for the exothermic peak representing the surface freezing under different cooling rate (Figure 3c), which proves that no phase separation is observed in the surface freezing phase.[22] Another reason causing the temperature deviation is probably due to the composition change in the surface freezing phase of binary *n*-alkane mixtures with large Δn in microcapsules. That is, the composition of surface freezing phase is different from that of bulk mixtures. As calculated using the molar fraction, the original composition of C_{18}/C_{22} is 1.97:1.61, while the composition of surface freezing phase varies to 2.12:1.41 in microcapsules. It means that the molar fraction of the shorter component is increased, and more molecules with the short carbon chain enter into the surface freezing phase, leading to small $\bar{n}$ and low T_s.

It is reported that poor solubility and the solid−solid phase separation will emerge in the binary *n*-alkane mixtures when $\Delta n \geq 4$.[54,55] As the special crystallization behavior which emerges at a higher temperature than the freezing point, surface freezing is proved to share the same composition as the bulk mixture when Δn is small (Figure 4). When Δn grows larger, it is richer in the longer component than the bulk nearly for all concentrations (Figure 5, upper part), and no phase separation will be found in the surface freezing phase.[22] In the present system, according to the DSC traces of m-C_{17}/C_{21} under different cooling rates (Figure 3c), the absence of phase separation in the surface freezing phase is confirmed; however, the relatively lower experimental T_s than the calculated value implies a totally

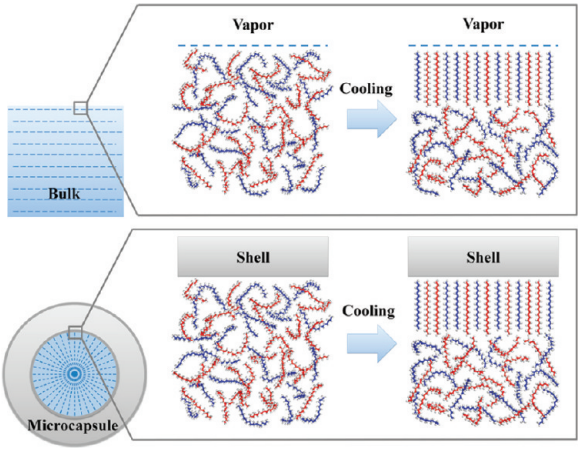

Figure 4. Schematic illustration of the crystal structure and interlayer arrangement of surface freezing phase of binary *n*-alkane mixtures with small Δn (1, 2, or 3). For both the bulk state (upper part) and microencapsulated state (lower part), the surface freezing phase shares the same composition with the mixture.

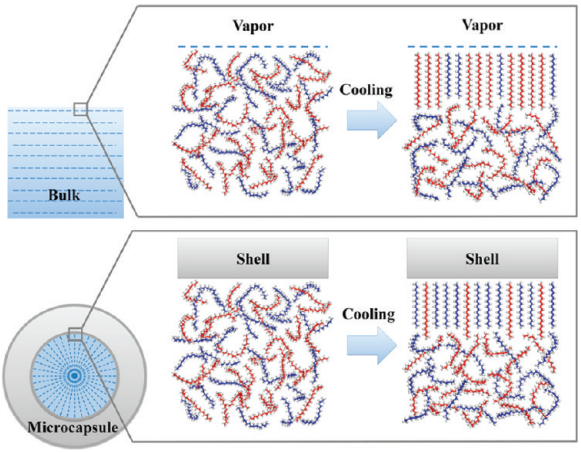

Figure 5. Schematic illustration of the crystal structure and interlayer arrangement of surface freezing phase of binary *n*-alkane mixtures with Δn = 4. For the bulk state (upper part), the surface crystalline monolayer is richer in the longer component than the bulk; while for the situation in microcapsules (lower part), the shorter component is enriched in the surface crystalline monolayer.

contrary situation in microcapsules that the shorter component is richer in the surface freezing phase (Figure 5, lower part). According to the literature, the layer structure (monolayer or bilayer) is dominant in surface freezing phase,[6] and the CH_3-terminated crystal face with low surface energy is regarded to play a decisive role in the formation of surface freezing phase.[19] In microcapsules, the specific surface area is dramatically larger than that in the bulk state, and hence the amount of the alkane molecules standing on the interface between the inner wall of microcapsules and the bulk mixture is greatly increased.[44] Compared with the molecules with the long carbon chain, the short ones will be more easily affected by the CH_3-terminated face, since the proportion of CH_3 group in the shorter component is larger than that of the longer one. Furthermore, the character change of the interface from the free state in bulk samples (liquid/vapor interface) to confined state in microcapsules (liquid/solid interface) may also contribute to the inversion of the enrichment. Hence, more alkane molecules with the short carbon chain will be "pulled" to approach the

dx.doi.org/10.1021/jp2125119 | J. Phys. Chem. B 2012, 116, 3099−3105

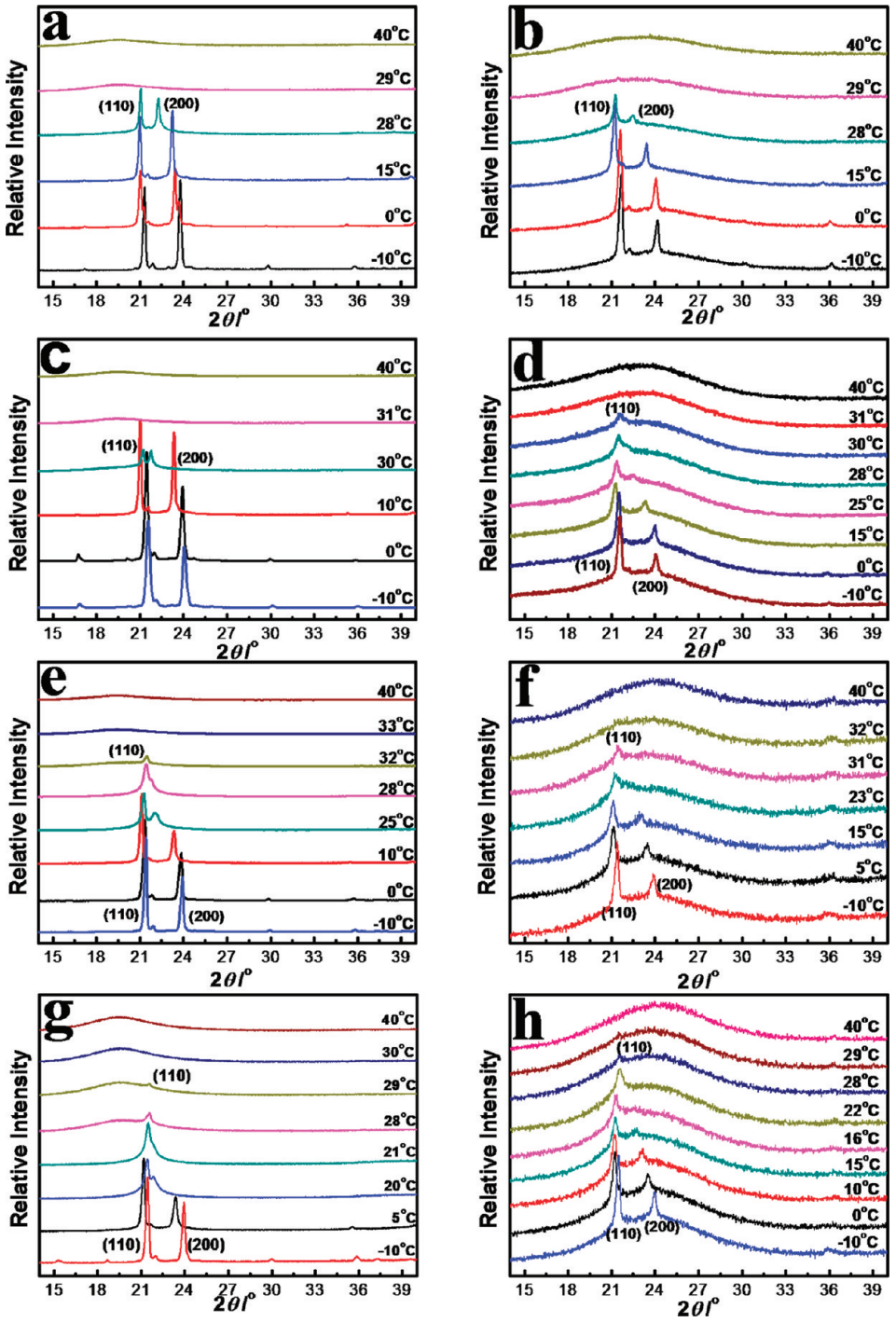

Figure 6. XRD results of the binary *n*-alkane mixtures during the cooling process: (a) bulk C_{18}/C_{19}; (b) *m*-C_{18}/C_{19}; (c) bulk C_{18}/C_{20}; (d) *m*-C_{18}/C_{20}; (e) bulk C_{18}/C_{21}; (f) *m*-C_{18}/C_{21}; (g) bulk C_{17}/C_{21}; (h) *m*-C_{17}/C_{21}. The cooling rate is 2 °C/min. At each temperature, all samples were equilibrated for about 5 min before measurements.

interface. When the temperature reaches T_s, the molecules on the interface will crystallize, and finally more *n*-alkane molecules with the short carbon chain enter the surface freezing phase, leading to smaller $\overline{n}$ and lower T_s.

Enhanced Stability of RII Phase. To further characterize the crystal structure and phase transitions during the crystallization process of all specimens, the temperature-dependent XRD measurements were performed, as shown in Figure 6. As mentioned above, RII is originally found in single *n*-alkanes (C_{22}–C_{26}) and binary alkane mixtures containing one or two of the above *n*-alkanes. Therefore, here we substitute C_{17}/C_{21}, with the same Δn, for C_{18}/C_{22}, in order to eliminate the influence of RII in C_{22}. As for $\Delta n = 1$ (Figure 6a,b), only the double characteristic diffraction peaks of (110) and (200) emerged during the cooling process of both samples. Those two peaks indicate the rotator phase I (abbreviated as RI) or the low-temperature ordered crystal phase, since they are both orthorhombic.[31] Therefore, RII does not emerge in these specimens. In contrast, RII emerged in the mixtures with larger Δn (3 and 4) both in the bulk state and in microcapsules (Figure 6e–h), characterized by

dx.doi.org/10.1021/jp2125119 | J. Phys. Chem. B 2012, 116, 3099–3105

the single diffraction peak at $2\theta = 21.6°$ at some certain temperatures.[31,44] For the medium $\Delta n = 2$ (C_{18}/C_{20}, Figure 6c,d), the situation is not as uniform as the above specimens. For the bulk C_{18}/C_{20} sample, RII was not detected. For the microencapsulated counterpart, however, RII emerged with a temperature region of 2 °C and then transferred to RI characterized by the double diffraction peaks, one for (110) near static and the other for (200) varying to larger 2θ value during the cooling process. The metastability of RII is also quite important, especially for the application of *n*-alkane mixtures as PCMs. Figure 7

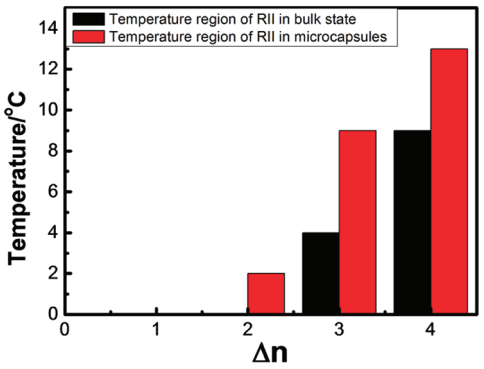

Figure 7. Temperature region of RII in the *n*-alkane and binary *n*-alkane mixtures both in the bulk state and in microcapsules. The RII crossover from transient to metastable is observed during the cooling process of *m*-C_{18}/C_{20}, showing a 2 °C temperature region, while no RII emerges during the cooling process of bulk C_{18}/C_{20}.

shows the temperature region for RII of all the specimens. Here C_{18} was added to form an integrated series for a detailed comparison since single *n*-alkanes can be regarded as the mixture with $\Delta n = 0$. Two tendencies are clearly illustrated, the first of which indicates that the larger the Δn becomes, the wider the metastable temperature region of RII is. This phenomenon was also observed before and attributed to the increase of disorder and the destruction of the layered structure in *n*-alkane mixtures.[32] The other one is referred to the 3D confinement, indicating that once microencapsulated, the metastable temperature region of RII could be greatly enlarged, and even the RII crossover from transient in the bulk state to metastable in microcapsules emerged (*m*-C_{18}/C_{20}).

In addition to the enhanced surface freezing phenomenon, the confined *n*-alkanes and their mixtures also exhibit some novel crystallization behaviors, such as the appearance of new rotator phases[44,45] or the suppression of solid−solid phase separations.[50,52] In microcapsules, the heterogeneous nucleation induced by the surface freezing phase has been proved to be dominant.[44] Since RII and RI have the same or similar in-planar arrangement as the surface freezing phase, the interface tension will be greatly reduced if these two rotator phases emerge in the liquid−rotator phase transition, thus resulting in the crossover of RII or RI from transient in the bulk state to metastable in the confinement. Here RII emerges in bulk binary mixtures with larger Δn but failed to emerge in *m*-C_{18}/C_{19} (Figure 6). The confined environment of *m*-C_{18}/C_{19} is nearly the same as that of other samples, where the surface freezing should be also equally enhanced, but RII is still absent as its bulk counterpart. In the bulk state, the surface freezing phenomenon can be also detected and then affect the subsequent crystallization.[23] However, since the amount of surface molecules is very small, the influence of the surface freezing phase is limited to a large extent. Therefore, without the enhanced surface freezing phenomenon RII still emerges in the samples with large Δn such as the bulk C_{18}/C_{21} and C_{17}/C_{21} during the cooling process. The appearance in bulk C_{18}/C_{21} and C_{17}/C_{21} and absence in *m*-C_{18}/C_{19} of RII imply that the enhanced surface freezing phenomenon is not essential for the RII crossover, while the interactions between the two components may decisively contribute to the emergence of RII. For *n*-alkane mixtures, the transition from RII to RI is the most common rotator−rotator phase transition.[32] These two rotator phases are both layered structure and have a similar in-planar arrangement, and the RII to RI transition is attributed to the alkane molecules approaching their next-nearest neighbors within the layer.[53] Hence, it is rationally supposed that if the orienting movement to the next-nearest neighbors could be suppressed, the RII to RI transition would be difficult to emerge, which makes RII more stable. Compare to the situation in single *n*-alkanes, the next-nearest neighbor of each molecule may belong to the other component for binary *n*-alkane mixtures, and the repulsion between the two molecules will be more intensive than that in single *n*-alkanes. With the enlargement of Δn for binary *n*-alkane mixtures, the molecular repulsion will be more enhanced, which will significantly suppress the alkane molecules approaching their next-nearest neighbors within the layer. Therefore, the rotator−rotator phase transition from RII to RI is more and more difficult, and RII can be stable in a large temperature region, even emerging in the bulk mixtures with larger Δn and microencapsulated mixtures with smaller Δn.

CONCLUSIONS

The crystallization behaviors of binary *n*-alkane mixtures with different carbon number difference (denoted as Δn) both in the bulk state and in microcapsules have been studied in the present investigation. The enhanced surface freezing phenomenon was also detected in all the microencapsulated samples, but the surface freezing temperature (T_s) of the mixture with $\Delta n = 4$ deviated from the predicted equation. The experimental T_s is 1 °C lower than the calculated value, which is attributed to the enrichment of alkane molecules with the short carbon chain in the surface freezing phase in the confinement. More short components are enriched on the interface between the inner wall of microcapsules and the bulk mixture, leading to the smaller average chain length in the surface freezing phase and lower T_s. Furthermore, the enlarging temperature region of RII in the binary *n*-alkane mixtures with increasing Δn is proved by XRD results, and even the crossover of RII from transient in the bulk state to metastable in microcapsules is observed during the cooling process of *m*-C_{18}/C_{20}. The enhanced surface freezing phenomenon can contribute to the enlargement, but it is the increasing molecular repulsion between the two components that suppresses the movement of molecules to the next-nearest neighbors and decisively affects the rotator−rotator phase transition from RII to RI, which finally causes the enlargement of the temperature region of RII. These findings may shed new light on the research and understanding of the phase change mechanism of PCMs consisting of *n*-alkanes or *n*-alkane mixtures.

AUTHOR INFORMATION

Corresponding Author

*Phone: +86-10-82618533; fax: +86-10-82612857; e-mail: ylsu@iccas.ac.cn (Y.S.), djwang@iccas.ac.cn (D.W.).

Notes

The authors declare no competing financial interest.

■ ACKNOWLEDGMENTS

We thank the National Natural Science Foundation of China (51103166) and China National Funds for Distinguished Young Scientists (Grant 50925313) for financial support.

■ REFERENCES

(1) Small, D. M. *The Physical Chemistry of Lipids*; Plenum: New York, 1986.
(2) Onder, E.; Sarier, N.; Cimen, E. *Thermochim. Acta* **2008**, *467*, 63−72.
(3) Jin, Z.; Wang, Y.; Liu, J.; Yang, Z. *Polymer* **2008**, *49*, 2903−2910.
(4) Ocko, B. M. *Phys. Rev. Lett.* **1990**, *64*, 2160−2163.
(5) Sirota, E. B.; Pershan, P. S.; Amador, S.; Sorensen, L. B. *Phys. Rev. A* **1987**, *35*, 2283−2287.
(6) Ocko, B. M.; Wu, X. Z.; Sirota, E. B.; Sinha, S. K.; Gang, O.; Deutsch, M. *Phys. Rev. E* **1997**, *55*, 3164−3182.
(7) Wu, X. Z.; Ocko, B. M.; Sirota, E. B.; Sinha, S. K.; Deutsch, M.; Cao, B. H.; Kim, M. W. *Science* **1993**, *261*, 1018−1021.
(8) Deutsch, M.; Wu, X. Z.; Sirota, E. B.; Sinha, S. K.; Ocko, B. M.; Magnussen, O. M. *Europhys. Lett.* **1995**, *30*, 283−288.
(9) Gang, O.; Ocko, B. M.; Wu, X. Z.; Sirota, E. B.; Deutsch, M. *Phys. Rev. Lett.* **1998**, *80*, 1264−1267.
(10) Wolf, S. G.; Leiserowitz, L.; Lahav, M.; Deutsch, M.; Kjaer, K.; Als-Nielsen, J. *Nature* **1987**, *328*, 63−66.
(11) Dutta, P.; Peng, J. B.; Lin, B.; Ketterson, J. B.; Prakash, M.; Georgopoulos, P.; Ehrlich, S. *Phys. Rev. Lett.* **1987**, *58*, 2228−2231.
(12) Wu, X. Z.; Ocko, B. M.; Sirota, E. B.; Sinha, S. K.; Deutsch, M. *Physica A* **1993**, *200*, 751−758.
(13) Wu, X. Z.; Sirota, E. B.; Sinha, S. K.; Ocko, B. M.; Deutsch, M. *Phys. Rev. Lett.* **1993**, *70*, 958−961.
(14) Gang, H.; Gang, O.; Shao, H. H.; Wu, X. Z.; Patel, J.; Hsu, C. S.; Deutsch, M.; Ocko, B. M.; Sirota, E. B. *J. Phys. Chem. B* **1998**, *102*, 2754−2758.
(15) Zhu, D. M.; Dash, J. G. *Phys. Rev. Lett.* **1986**, *57*, 2959−2962.
(16) Maeda, N.; Christenson, H. K. *Colloids Surf., A* **1999**, *159*, 135−148.
(17) Maeda, N.; Yaminshy, V. V. *Phys. Rev. Lett.* **2000**, *84*, 698−700.
(18) Lei, Q.; Bain, C. D. *Phys. Rev. Lett.* **2004**, *92*, 176103.
(19) Sirota, E. B.; Wu, X. Z.; Ocko, B. M.; Deutsch, M. *Phys. Rev. Lett.* **1997**, *79*, 531−531.
(20) Tkachenko, A. V.; Rabin, Y. *Phys. Rev. Lett.* **1996**, *76*, 2527−2530.
(21) Wu, X. Z.; Ocko, B. M.; Deutsch, M.; Sirota, E. B.; Sinha, H. A. *Physica B* **1996**, *221*, 261−266.
(22) Sloutskin, E.; Wu, X. Z.; Peterson, T. B.; Gang, O.; Ocko, B. M.; Sirota, E. B.; Deutsch, M. *Phys. Rev. E* **2003**, *68*, 031605.
(23) Sloutskin, E.; Sirota, E. B.; Kraack., H.; Ocko, B. M.; Deutsch, M. *Phys. Rev. E* **2001**, *64*, 031708.
(24) Sear, R. P. *Langmuir* **2002**, *18*, 7571−7576.
(25) Sirota, E. B. *J. Chem. Phys.* **2000**, *112*, 492−500.
(26) Sloutskin, E.; Sirota, E. B.; Gang, O.; Wu, X. Z.; Ocko, B. M.; Deutsch, M. *Eur. Phys. J. E* **2004**, *13*, 109−112.
(27) Sirota, E. B.; King, H. E. Jr.; Singer, D. M.; Shao, H. H. *J. Chem. Phys.* **1993**, *98*, 5809−5824.
(28) Ungar, G. *J. Phys. Chem.* **1983**, *87*, 689−695.
(29) Sirota, E. B.; Singer, D. M. *J. Chem. Phys.* **1994**, *101*, 10873−10882.
(30) Doucet, J.; Denicolo, I.; Craievich, A.; Collet, A. *J. Chem. Phys.* **1981**, *75*, 5125−5127.
(31) Dirand, M.; Bouroukba, M.; Chevallier, V.; Petitjean, D. *J. Chem. Eng. Data* **2002**, *47*, 115−143.
(32) Sirota, E. B.; King, H. E.; Shao, H. H.; Singer, D. M. *J. Phys. Chem.* **1995**, *99*, 798−804.
(33) Nozue, Y.; Kawashima, Y.; Seno, S.; Nagamatsu, T.; Hosoda, S.; Berda, E. B.; Rojas, G.; Baughman, T. W.; Wagener, K. B. *Macromolecules* **2011**, *44*, 4030−4034.
(34) Massa, M. V.; Carvalho, J. L.; Dalnoki-Veress, K. *Eur. Phys. J. E* **2003**, *12*, 111−117.
(35) Jin, Y.; Rogunova, M.; Hiltner, A.; Baer, E.; Nowacki, R.; Galeski, A.; Piorkowska, E. *J. Polym. Sci., Polym. Phys.* **2004**, *42*, 3380−3396.
(36) Berwanger, R.; Henschel, A.; Knorr, K.; Huber, P.; Pelster, R. *Phys. Rev. B* **2009**, *79*, 125442.
(37) Gruener, S.; Huber, P. *Phys. Rev. Lett.* **2009**, *103*, 174501.
(38) Kusmin, A.; Gruener, S.; Henschel, A.; Holderer, O.; Allgaier, J.; Richter, D.; Huber, P. *J. Phys. Chem. Lett.* **2010**, *1*, 3116−3121.
(39) Kalyanasundaram, V.; Spearot, D. E.; Malshe, A. P. *Langmuir* **2009**, *25*, 7553−7560.
(40) Singh, S. K.; Sinha, A.; Deo, G.; Singh, J. K. *J. Phys. Chem. C* **2009**, *113*, 7170−7180.
(41) Cai, T.; Qian, Y.; Ma, Y.; Ren, Y.; Hu, W. *Macromolecules* **2009**, *42*, 3381−3385.
(42) Hu, W.; Cai, T.; Ma, Y.; Hobbs, J. K.; Farrance, O.; Reiter, G. *Faraday Discuss.* **2009**, *143*, 129−141.
(43) Gehlsen, M. D.; Bates, F. S. *Macromolecules* **1993**, *26*, 4122−4127.
(44) Xie, B.; Shi, H.; Jiang, S.; Zhao, Y.; Han, C. C.; Xu, D.; Wang, D. *J. Phys. Chem. B* **2006**, *110*, 14279−14282.
(45) Xie, B.; Shi, H.; Liu, G.; Zhou, Y.; Wang, Y.; Zhao, Y.; Wang, D. *J. Phys. Chem. B* **2008**, *112*, 13310−13315.
(46) Fu, D.; Su, Y.; Xie, B.; Zhu, H.; Liu, G.; Wang, D. *Phys. Chem. Chem. Phys.* **2011**, *13*, 2021−2025.
(47) Xie, B.; Shi, H.; Liu, G.; Zhou, Y.; Wang, Y.; Zhao, Y.; Wang, D. *Chem. Mater.* **2008**, *20*, 3099−3104.
(48) Liu, G.; Xie, B.; Fu, D.; Wang, Y.; Fu, Q.; Wang, D. *J. Mater. Chem.* **2009**, *19*, 6605−6609.
(49) Fu, D.; Su, Y.; Xie, B.; Liu, G.; Li, Z.; Jiang, K.; Wang, D. *Colloids Surf., A* **2011**, *384*, 219−227.
(50) Jiang, K.; Su, Y.; Xie, B.; Jiang, S.; Zhao, Y.; Wang, D. *J. Phys. Chem. B* **2008**, *112*, 16485−16489.
(51) Jiang, K.; Su, Y.; Xie, B.; Meng, Y.; Wang, D. *J. Phys. Chem. B* **2009**, *113*, 3269−3272.
(52) Fu, D.; Liu, Y.; Su, Y.; Liu, G.; Wang, D. *J. Phys. Chem. B* **2011**, *115*, 4632−4638.
(53) Fu, D.; Liu, Y.; Liu, G.; Su, Y.; Wang, D. *Phys. Chem. Chem. Phys.* **2011**, *13*, 15031−15036.
(54) Synder, R. G.; Gob, M. C.; Srivatsavoy, V. J. P.; Straw, H. L.; Dorset, D. L. *J. Phys. Chem.* **1992**, *96*, 10008−10019.
(55) Annis, B. K.; Londono, J. D.; Wignall, G. D.; Snyder, R. G. *J. Phys. Chem.* **1996**, *100*, 1725−1730.
(56) Hacura, A.; Kaczorowska, B. *J. Mol. Struct.* **2005**, *744*, 581−584.